Available online at www.sciencedirect.com
SCIENCE DIRECT®
Journal of Sound and Vibration 284 (2005) 757–781
JOURNAL OF SOUND AND VIBRATION
www.elsevier.com/locate/jsvi

# Identification of stiffness and damping properties of thin isotropic vibrating plates using the virtual fields method: theory and simulations

Alain Giraudeau*, Fabrice Pierron

*Laboratoire de Mécanique et Procédés de Fabrication (JE 2381), Ecole Nationale Supérieure d'Arts et Métiers, Rue Saint-Dominique, BP 508, 51006 Châlons-en-Champagne Cedex, France*

Received 17 November 2003; received in revised form 12 March 2004; accepted 13 July 2004
Available online 15 December 2004

**Abstract**

The present paper proposes a novel procedure to derive both stiffness and damping parameters from forced vibrating isotropic plates. The key feature is that displacement and curvature fields can be measured at different times over the whole surface of the plate by a suitable optical technique. As a consequence, the virtual fields method (VFM) provides sets of equations relating the stiffness and damping parameters to these measured fields and to geometric and excitation (frequency, amplitude) parameters. First, the theory of the VFM is exposed and, then, validation is performed on simulated full-field displacement and curvature data. Calculations are performed in the case of isotropic plates with low and high damping, at resonance and out of resonance. It is shown that the procedure is valid and robust to noise, except on the damping parameters when the damping is low. Future work necessary to develop the method is described as a conclusion.


## 1. Introduction

The measurement of material elastic stiffness parameters, essential for predicting the behaviour of structures, is common in material-testing laboratories. It is usually performed using tension,

*Corresponding author. Tel.: +33 326699112; fax: +33 326699114.
*E-mail address:* alain.giraudeau@chalons.ensam.fr (A. Giraudeau).

0022-460X/$ - see front matter © 2004 Elsevier Ltd. All rights reserved.
doi:10.1016/j.jsv.2004.07.009

bending or torsion tests on rectangular coupons, leading to simple stress states that can be expressed as functions of the specimen geometry and the applied load through a closed-form solution of the mechanical problem. Nevertheless, these procedures exhibit certain drawbacks. First, experimental boundary conditions must comply with that of the mechanical model, which is not always easy to achieve, particularly for anisotropic materials for which the usual Saint-Venant assumption for isotropic materials is no longer valid [1,2]. Moreover, anisotropic coupling effects can cause specific testing difficulties [3]. Finally, only a small number of parameters can be retrieved from a specific test because of the very simple stress state. As a result, several tests have to be performed usually to identify the full set of material parameters, increasing the cost of the procedure.

An alternative to these usual testing procedures is to consider more complex configurations for which the constraints on the boundary conditions will be less severe, since in this case the stress state is unknown a priori and no closed-form solution is available. Moreover, since all stress components are present in this case, it can be expected that a greater number of material parameters will be involved in the response of the specimen and can therefore be measured. In this case, new strategies are to be developed to extract the material stiffnesses. Such approaches have been implemented using the eigen-frequencies of vibrating plates, coupled to some numerical procedure based on finite element model updating [4–9] or some approximation of the solution [10,11]. An alternative to these methods was suggested by Grédiac et al., making use of the measurement of slope fields at the surface of bent plates [12–14] and performing the identification through the so-called Virtual Fields Method (VFM). The main advantage of this technique is that stiffnesses are obtained directly (no iterations, no optimization scheme) and that constraints on specimen geometry and boundary conditions are less critical.

The problem of the measurement of damping parameters is more acute. Indeed, although such information is necessary to perform accurate simulation of the vibrations of a large range of structures (for instance, to compute the forces in joints or the vibro-acoustic response of a car), fewer research efforts have been dedicated to this. Moreover, damping parameters have proved more tricky to measure than stiffnesses because of all the parasitic dissipation that is usually added in a classical mechanical test. Most of the work encountered in the literature concerns beam specimens. A usual strategy consists in monitoring the vibrations of beams in free vibrations, either in bending with free–free or cantilever boundary conditions [15–20], in torsion [21,22] or in longitudinal vibrations [23]. The results are processed using either the logarithmic decay time when the first mode is predominant [15,16,18–20,22] or the width of the $-3$ dB peak of the impulse response in the frequency domain when several modes are present. Other techniques such as circle-fit in the Argand plane can also be found [24]. Some authors prefer to work on forced vibrating beams [25,26], using inertial excitation [25] or clamped–clamped beams with mid-span loading [26]. In any case, the experimental problems encountered by the authors are often similar: dissipation coming from the boundary conditions [16,19], presence of higher order modes [18].

The purpose of the present paper is to propose a novel procedure to extract both stiffness and damping parameters from forced vibrating plates. It is an extension of initial work by Grédiac et al. [12,13] using the VFM, where damping was not considered. This study shows how damping can be introduced in the VFM procedure.

## 2. Theory

For a solid of any shape, in the case of small perturbations and absence of volume forces, the general expression of the principle of virtual work can be written as

$$-\int_V \sigma : \varepsilon^* \, \mathrm{d}V + \int_{\partial V} F.u^* \, \mathrm{d}S = \int_V a.u^* \, \mathrm{d}m, \tag{1}$$

where $\sigma$ is the stress tensor, $\varepsilon^*$ is a virtual strain tensor, $V$ is the volume of the solid, $\partial V$ the surface of its boundary, $F$ the surface density of external forces acting on $\partial V$, $u^*$ is a kinematically admissible virtual displacement field associated to $\varepsilon^*$, $a$ is the acceleration field, $\mathrm{d}V$, $\mathrm{d}S$ and $\mathrm{d}m$ are, respectively, elementary volume, surface and mass.

The principle of the VFM is to replace the stress components in the above equation by the true elastic strains through the constitutive equations of which parameters are to be identified. Then, by selecting 'appropriate' virtual fields, it is possible to derive equations relating the materials constitutive parameters to integral functions of the true strains. If full-field measurements are available, then these integral functions can be evaluated and, if enough independent virtual fields are used, the materials constitutive parameters can be identified. In the present section, it is shown how this method can be adapted to damping identification.

### 2.1. Considered case

Let us consider now that the solid is a rectangular thin plate. Its thickness is $h$ (Fig. 1).

The plate is clamped at point $O$ as seen in Fig. 1, which is the origin of the coordinate system. Let us now suppose that this point is translated along the $z$-axis in a sine movement (inertial excitation). This arrangement is an extension of the experimental study of vibrating plates reported in Ref. [27]. If we call $\delta(t)$ the displacement of this point along the $z$-direction, and using usual complex notations, then:

$$\delta(t) = d \cos \omega t = \mathrm{Re}(d \exp(\mathrm{j}\omega t)), \tag{2}$$

where $\omega$ is the pulsation and $d$ the amplitude of the sine movement. For a homogeneous material, this is a case of pure bending and only out-of-plane displacements will be considered. Assuming classical thin plate theory, they are independent on $z$. The global out-of-plane displacement field $\mu(x, y, t)$ is therefore the superposition of the imposed excitation displacement $\delta(t)$ and the

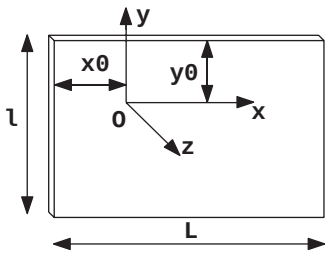


Fig. 1. Rectangular plate under study.

out-of-plane deflection $\lambda(x, y, t)$ due to the deformation of the plate:

$$\mu(x, y, t) = \delta(t) + \lambda(x, y, t). \tag{3}$$

The deflection caused by the deformation of the plate is made up of the combination of the response of each mode:

$$\mu(x, y, t) = \delta(t) + \sum_{k=1}^{\infty} \lambda_k(x, y, t), \tag{4}$$

where $\lambda_k(x, y, t)$ is the response of the $k$th mode. Since the excitation has a sine shape and assuming the linear behaviour of the plate, the response is harmonic with the same pulsation $\omega$:

$$\mu(x, y, t) = \delta(t) + \sum_{k=1}^{\infty} |\lambda_k(x, y)| \cos(\omega t - \phi_k(x, y)), \tag{5}$$

where $|\lambda_k(x, y)|$ and $\phi_k(x, y)$ are, respectively, the amplitude and the phase of the response of the $k$th mode. Because of the damping, the latter can take all the values between 0 and $\pi$, depending on the distance between the excitation and the $k$th mode frequency. In the case of a plate having sufficiently separated modes and excited close to its $k$th mode frequency, the response is dominated by that of the resonant mode whose amplitude becomes predominant and whose phase comes close to $\pi/2$. The responses linked to the other modes have relatively small amplitudes and their phases are close to 0 or $\pi$. One could therefore think that, in this case, their contributions could be ignored. In fact, this is not always the case and it depends on the considered mode and on the importance of the damping.

In the general case, a correct representation of the harmonic response of the vibrating plate must take into account the contributions of a great number of modes even close to a resonance and even with well-separated modal frequencies. Using complex notation, it is more convenient to write

$$\begin{aligned} \mu(x, y, t) &= \mathrm{Re}(u(x, y) \exp(\mathrm{j}\omega t)) \\ &= \mathrm{Re}((d + w(x, y)) \exp(\mathrm{j}\omega t)), \end{aligned} \tag{6}$$

with

$$\begin{aligned} &u(x, y) \in \mathbb{C}, \quad u(x, y) = u_r(x, y) + \mathrm{j}u_i(x, y), \\ &w(x, y) \in \mathbb{C}, \quad w(x, y) = w_r(x, y) + \mathrm{j}w_i(x, y). \end{aligned} \tag{7}$$

These expressions for $u(x, y)$ and $w(x, y)$ provide complete representations of the harmonic responses and are valid regardless of the excitation frequency (physical basis as opposed to the modal basis).

### 2.2. Choice of the virtual fields

The virtual displacement fields must be kinematically admissible. In particular, it means that they should be such that the virtual movement of point $O$ matches its true movement. For instance, they can be written as

$$u^*(x, y) \exp(\mathrm{j}\omega t) = (d + w^*(x, y)) \exp(\mathrm{j}\omega t), \quad u^*(x, y) \in \mathbb{C}, \ w^*(x, y) \in \mathbb{C}, \tag{8}$$

with

$$u^*(x,y) = u_r^*(x,y) + \mathrm{j}u_i^*(x,y) = d + w_r^*(x,y) + \mathrm{j}w_i^*(x,y), \tag{9}$$

where $w^*(x,y) = w_r^*(x,y) + \mathrm{j}w_i^*(x,y)$ is a virtual deflection field, with $w^*(0,0) = 0$. As mentioned in Section 2.3, $w^*$ must be such that the clamping moments do not work virtually. Therefore, one must have

$$\frac{\partial w^*}{\partial x}(0,0) = 0 \quad \text{and} \quad \frac{\partial w^*}{\partial y}(0,0) = 0. \tag{10}$$

It is interesting to note that, in practice, the clamping will not be reduced to one point but to a small area of the plate (area under the head of a nut, for instance). In this case, it will be necessary to extend the above condition to the whole area. A way of doing this could be to use piecewise virtual fields with a rigid-body virtual field over a square area containing the constrained material. Such piecewise virtual fields are presently under development [28].

### 2.3. Virtual work of external forces

The only external forces acting on the plate are those introduced by the clamping at point $O$ (see Fig. 1). If there is a chance to measure experimentally the force acting in the $z$-direction, the two bending moments $M_x$ and $M_y$ will be unknown and their contribution to the virtual work of the external forces will have to be zeroed by choosing appropriate virtual fields (see Section 2.2). Let us consider now only $F$, the force in the $z$-direction. It can be written as

$$F\ \exp(\mathrm{j}\omega t) = (F_r + \mathrm{j}F_i)\ \exp(\mathrm{j}\omega t). \tag{11}$$

Therefore, the virtual work of the external forces (VWEF) can be simply written as

$$\mathrm{VWEF} = \mathrm{Re}(F\ \exp(\mathrm{j}\omega t))\,\mathrm{Re}(d\ \exp(\mathrm{j}\omega t)). \tag{12}$$

Developing the above, it can be shown that

$$\mathrm{VWEF} = \tfrac{1}{2}F_r d + \tfrac{1}{2}\mathrm{Re}(Fd\ \exp(\mathrm{j}2\omega t)). \tag{13}$$

Finally, we get

$$\mathrm{VWEF} = \tfrac{1}{2}F_r d + \tfrac{1}{2}F_r d\ \cos(2\omega t) - \tfrac{1}{2}F_i d\ \sin(2\omega t). \tag{14}$$

It can be seen that VWEF is composed of three distinct terms, one independent of time and the two others depending on sine and cosine of twice the excitation pulsation.

### 2.4. Virtual work of the internal forces

The virtual work of the internal forces (VWIF) is written according to the Love-Kirchhoff theory of thin plates [29]. In the case of dissipative materials, VWIF can be written as the sum of an elastic and a dissipative contribution. One has

$$\mathrm{VWIF} = -\int_S (\{m^e\} + \{m^d\})\{\kappa\}^*\,\mathrm{d}S, \tag{15}$$

where $\{m^e\}$ and $\{m^d\}$ are, respectively, the elastic and dissipative moments and $\{\kappa\}^*$ is the virtual curvature field resulting from the virtual displacement field described in Section 2.2. It is important to note at this stage that the three above quantities are complex.

In the case of an isotropic and homogeneous material, the elastic moment can be written as

$$\{m^e\} = \begin{bmatrix} m_x^e \\ m_y^e \\ m_s^e \end{bmatrix} = \begin{bmatrix} D_{xx} & D_{xy} & 0 \\ D_{xy} & D_{xx} & 0 \\ 0 & 0 & (D_{xx} - D_{xy})/2 \end{bmatrix} \cdot \begin{bmatrix} k_x \\ k_y \\ k_s \end{bmatrix}, \tag{16}$$

where $D_{xx}$ and $D_{xy}$ are the isotropic bending stiffness components of the plate.

Assuming that the dissipation is viscous and that the isotropic bending dissipation components of the plate, $B_{xx}$ and $B_{xy}$, are proportional to the elastic ones, one can write

$$\{m^d\} = \begin{bmatrix} m_x^d \\ m_y^d \\ m_s^d \end{bmatrix} = \begin{bmatrix} B_{xx} & B_{xy} & 0 \\ B_{xy} & B_{xx} & 0 \\ 0 & 0 & (B_{xx} - B_{xy})/2 \end{bmatrix} \cdot \frac{\partial}{\partial t} \begin{bmatrix} k_x \\ k_y \\ k_s \end{bmatrix}. \tag{17}$$

Since the response of the plate is harmonic of pulsation $\omega$, one has $(\partial/\partial t)\{\kappa\} = \mathrm{j}\omega\{\kappa\}$ and finally we get

$$\{m^d\} = \begin{bmatrix} m_x^d \\ m_y^d \\ m_s^d \end{bmatrix} = \mathrm{j}\omega \cdot \begin{bmatrix} B_{xx} & B_{xy} & 0 \\ B_{xy} & B_{xx} & 0 \\ 0 & 0 & (B_{xx} - B_{xy})/2 \end{bmatrix} \cdot \begin{bmatrix} k_x \\ k_y \\ k_s \end{bmatrix}. \tag{18}$$

It is important to note that the method could be used with other formulations of damping. The one chosen here is kept as simple as possible to demonstrate the method. It can be shown that Eq. (15) can be written as

$$\begin{aligned} \mathrm{VWIF} = {} & \tfrac{1}{2}\mathrm{Re}\left(\int_S (\{m^e\} + \{m^d\})\{\overline{\kappa}\}^* \,\mathrm{d}S\right) \\ & + \tfrac{1}{2}\mathrm{Re}\left(\int_S (\{m^e\} + \{m^d\})\{\kappa\}^* \exp(\mathrm{j}2\omega t)\,\mathrm{d}S\right), \end{aligned} \tag{19}$$

where $\{\overline{\kappa}\}^*$ indicates the conjugate of the virtual curvatures.

Using Eqs. (16) and (17) to replace in Eq. (19), one can define the quantities $G_{p,q}$ and $H_{p,q}$ such that

$$\begin{aligned} G_{p,q} &= -\int_S \left(k_x(x,y)k_x^* + k_y(x,y)k_y^* + \tfrac{1}{2}k_s(x,y)k_s^*\right)\mathrm{d}S, \\ H_{p,q} &= -\int_S \left(k_x(x,y)k_y^* + k_y(x,y)k_x^* - \tfrac{1}{2}k_s(x,y)k_s^*\right)\mathrm{d}S, \end{aligned} \tag{20}$$

where $p$ and $q$ indicate that the $G_{p,q}$ and $H_{p,q}$ quantities are calculated using:

- the real or imaginary parts of the actual curvatures according to whether $p$ is $r$ or $i$;
- the real or imaginary parts of the virtual curvatures according to whether $q$ is $r$ or $i$.

For instance, $G_{i,r}$ can be written as

$$G_{i,r} = -\int_S \left( k_{x_i}(x,y)k^*_{x_r} + k_{y_i}(x,y)k^*_{y_r} + \tfrac{1}{2}k_{s_i}(x,y)k^*_{s_r} \right) \mathrm{d}S. \tag{21}$$

Therefore, VWIF can be expressed using four $G$ quantities: $G_{r,r}$, $G_{i,i}$, $G_{i,r}$, $G_{r,i}$ and four $H$ quantities: $H_{r,r}$, $H_{i,i}$, $H_{i,r}$, $H_{r,i}$.

Finally, one has

$$\begin{aligned}\mathrm{VWIF} = {} & \tfrac{1}{2}[D_{xx}(G_{r,r} + G_{i,i}) + D_{xy}(H_{r,r} + H_{i,i})] \\ & + \tfrac{1}{2}[B_{xx}\omega(G_{r,i} - G_{i,r}) + B_{xy}\omega(H_{r,i} - H_{i,r})] \\ & + \tfrac{1}{2}[D_{xx}(G_{r,r} - G_{i,i}) + D_{xy}(H_{r,r} - H_{i,i})]\cos(2\omega t) \\ & + \tfrac{1}{2}[-B_{xx}\omega(G_{i,r} + G_{r,i}) - B_{xy}\omega(H_{i,r} + H_{r,i})]\cos(2\omega t) \\ & - \tfrac{1}{2}[D_{xx}(G_{r,i} + G_{i,r}) + D_{xy}(H_{r,i} + H_{i,r})]\sin(2\omega t) \\ & - \tfrac{1}{2}[B_{xx}\omega(G_{r,r} - G_{i,i}) + B_{xy}\omega(H_{r,r} - H_{i,i})]\sin(2\omega t).\end{aligned} \tag{22}$$

### 2.5. Virtual work of the inertial forces

Taking into account Eq. (7), the acceleration $a$ can be written as

$$\begin{aligned}a(x,y)\exp(\mathrm{j}\omega t) &= \frac{\partial^2}{\partial t^2}(u(x,y)\exp(\mathrm{j}\omega t)) \\ &= -\mathrm{d}\omega^2\exp(\mathrm{j}\omega t) - w(x,y)\omega^2\exp(\mathrm{j}\omega t).\end{aligned} \tag{23}$$

Moreover, $\mathrm{d}m = \rho h\,\mathrm{d}S$, where $\rho$ is the density of the material. Therefore, the virtual work of the inertial forces VWAC can be written as

$$\begin{aligned}\mathrm{VWAC} = {} & -\frac{\rho h\omega^2}{2}\,\mathrm{Re}\left(\int_S u(x,y)\overline{u}^*(x,y)\,\mathrm{d}S\right) \\ & -\frac{\rho h\omega^2}{2}\,\mathrm{Re}\left(\int_S u(x,y)u^*(x,y)\exp(\mathrm{j}2\omega t)\,\mathrm{d}S\right),\end{aligned} \tag{24}$$

where $\overline{u}^*(x,y)$ indicates the conjugate of the virtual displacement field. Finally, we get

$$\begin{aligned}\mathrm{VWAC} = {} & -\frac{\rho h\omega^2}{2}\int_S (u_r u_r^* + u_i u_i^*)\,\mathrm{d}S \\ & -\frac{\rho h\omega^2}{2}\int_S (u_r u_r^* - u_i u_i^*)\,\mathrm{d}S\cos(2\omega t) \\ & +\frac{\rho h\omega^2}{2}\int_S (u_r u_i^* + u_i u_r^*)\,\mathrm{d}S\sin(2\omega t).\end{aligned} \tag{25}$$

### 2.6. Summary

Following the above calculations, the principle of virtual work can be written as

$$\mathrm{VWIF} + \mathrm{VWEF} = \mathrm{VWAC}, \tag{26}$$

with the expressions for VWIF, VWEF and VWAC given in the previous sections. As shown previously, each contribution is written as the sum of a term independent of time and two terms dependent on sine and cosine of twice the excitation pulsation. Since the above equality is verified for any time, it can be split into three separate equations. Moreover, the expressions are valid for any combination of the real and imaginary parts of the virtual fields. As a consequence, each of the three equations can again be split into two equations, leading finally to a system of six equations, out of which only four are independent. These equations are given below:

$$D_{xx}G_{r,r} + D_{xy}H_{r,r} - B_{xx}\omega G_{i,r} - B_{xy}\omega H_{i,r} + F_r d = -\rho h\omega^2 \int_S u_r u_r^* \,\mathrm{d}S, \tag{27}$$

$$D_{xx}G_{i,i} + D_{xy}H_{i,i} + B_{xx}\omega G_{r,i} + B_{xy}\omega H_{r,i} = -\rho h\omega^2 \int_S u_i u_i^* \,\mathrm{d}S, \tag{28}$$

$$D_{xx}G_{i,r} + D_{xy}H_{i,r} + B_{xx}\omega G_{r,r} + B_{xy}\omega H_{r,r} + F_i d = -\rho h\omega^2 \int_S u_i u_r^* \,\mathrm{d}S, \tag{29}$$

$$D_{xx}G_{r,i} + D_{xy}H_{r,i} - B_{xx}\omega G_{i,i} - B_{xy}\omega H_{i,i} = -\rho h\omega^2 \int_S u_r u_i^* \,\mathrm{d}S. \tag{30}$$

Since $u(x,y) = d + w_r(x,y) + \mathrm{j}w_i(x,y)$ and $u^*(x,y) = d + w_r^*(x,y) + \mathrm{j}w_i^*(x,y)$, $w_r^*(x,y)$ can be taken as zero in Eqs. (27) and (29), which corresponds to a virtual rigid body movement. In this case, the two force components can be extracted directly:

$$F_r = -\rho h\omega^2 \int_S (d + w_r) \,\mathrm{d}S, \tag{31}$$

$$F_i = -\rho h\omega^2 \int_S w_i \,\mathrm{d}S. \tag{32}$$

This leaves the following four equations:

$$D_{xx}G_{r,r} + D_{xy}H_{r,r} - B_{xx}\omega G_{i,r} - B_{xy}\omega H_{i,r} = -\rho h\omega^2 \int_S (d + w_r) w_r^* \,\mathrm{d}S, \tag{33}$$

$$D_{xx}G_{i,i} + D_{xy}H_{i,i} + B_{xx}\omega G_{r,i} + B_{xy}\omega H_{r,i} = -\rho h\omega^2 \int_S w_i w_i^* \,\mathrm{d}S, \tag{34}$$

$$D_{xx}G_{r,i} + D_{xy}H_{r,i} - B_{xx}\omega G_{i,i} - B_{xy}\omega H_{i,i} = -\rho h\omega^2 \int_S (d + w_r) w_i^* \,\mathrm{d}S, \tag{35}$$

$$D_{xx}G_{i,r} + D_{xy}H_{i,r} + B_{xx}\omega G_{r,r} + B_{xy}\omega H_{r,r} = -\rho h\omega^2 \int_S w_i w_r^* \,\mathrm{d}S. \tag{36}$$

These four equations are symmetrical with respect to the real and imaginary parts of the virtual deflection field. Therefore, it is equivalent to using these four equations with $u^*(x,y) = d + w_r^*(x,y) + \mathrm{j}w_i^*(x,y)$, with $w_r^*(x,y) \neq w_i^*(x,y)$, or to use the two first ones, Eqs. (33) and (34), with the two virtual fields: $u_1^*(x,y) = d + w_r^*(x,y)(1+j)$ and $u_2^*(x,y) = d + w_i^*(x,y)(1+j)$, with $w_r^*(x,y) \neq w_i^*(x,y)$. Therefore, only Eqs. (33) and (34) will be kept in the following.

### 2.7. Interpretation

When the excitation has a frequency very close to the frequency of a mode, this latter is resonant. Its contribution, which lags at $\pi/2$ with respect to the driving movement, could be predominant in the response of the plate and mainly represented by the imaginary part of the deflection $w_i(x,y)$. The responses of the other modes are mainly contained in the real part $w_r(x,y)$ and can be much smaller than the imaginary one.

Assuming $w_r(x,y)$ is negligible compared to $w_i(x,y)$, one can write

$$w_r(x,y) \simeq 0, \quad u_r(x,y) \simeq d, \quad u_i(x,y) = w_i(x,y). \tag{37}$$

Therefore, the real part of the curvatures is close to zero, so that the four quantities $G_{r,r}, G_{r,i}, H_{r,r}$ and $H_{r,i}$ are also close to zero. With these approximations, simplified versions of Eqs. (33), (34), (31) and (32) can be written as

$$B_{xx}G_{i,r} + B_{xy}H_{i,r} = -\rho h\omega \int_S (d + w_r) w_r^* \, \mathrm{d}S, \tag{38}$$

$$D_{xx}G_{i,i} + D_{xy}H_{i,i} = -\rho h\omega^2 \int_S w_i w_i^* \, \mathrm{d}S, \tag{39}$$

$$F_r = -\rho h\omega^2 d \int_S \mathrm{d}S, \tag{40}$$

$$F_i = -\rho h\omega^2 \int_S w_i \, \mathrm{d}S. \tag{41}$$

These approximated equations only work with the contribution of the resonant mode. Eq. (39) shows the equilibrium between the elastic forces and the acceleration forces. Eq. (38) shows that, at resonance, the work provided by the driving movement is balanced by the internal dissipation of the plate. Eq. (40) simply states that the in-phase clamping force is equal to the inertial force of the undeformed plate. This is normal, since at resonance there is no in-phase deformation of the plate. Finally, Eq. (41) describes the clamping force when the plate is back at its equilibrium position and the only deflections come from the deformation of the plate.

### 2.8. Resolution

In the general case, four quantities are to be identified: $D_{xx}, D_{xy}, B_{xx}, B_{xy}$. It is assumed that the real and imaginary parts of the deflection and the curvatures are provided by the full-field measurement technique, capturing the in-phase and out-of-phase ($\pi/2$ lag) responses of the

vibrating plate. Two independent virtual fields $u^*_{(1)}$ and $u^*_{(2)}$ can be chosen, such that

$$u^*_{(1)} = d + w^*_{r(1)} + \mathrm{j}w^*_{i(1)}, \quad u^*_{(2)} = d + w^*_{r(2)} + \mathrm{j}w^*_{i(2)}. \tag{42}$$

With the actual curvatures, the $G^{(1)}_{p,q}$ and $H^{(1)}_{p,q}$ quantities are derived from the first virtual field, and the $G^{(2)}_{p,q}$ and $H^{(2)}_{p,q}$ ones are derived from the second. Then, introducing successively the expressions of these two virtual fields in Eqs. (33) and (34) leads to a set of four linear independent equations, which is written below in matrix form:

$$\begin{bmatrix} G^{(1)}_{i,i} & H^{(1)}_{i,i} & \omega G^{(1)}_{r,i} & \omega H^{(1)}_{r,i} \\ G^{(1)}_{r,r} & H^{(1)}_{r,r} & -\omega G^{(1)}_{i,r} & -\omega H^{(1)}_{i,r} \\ G^{(2)}_{i,i} & H^{(2)}_{i,i} & \omega G^{(2)}_{r,i} & \omega H^{(2)}_{r,i} \\ G^{(2)}_{r,r} & H^{(2)}_{r,r} & -\omega G^{(2)}_{i,r} & -\omega H^{(2)}_{i,r} \end{bmatrix} \cdot \begin{bmatrix} D_{xx} \\ D_{xy} \\ B_{xx} \\ B_{xy} \end{bmatrix} = \begin{bmatrix} -\rho h\omega^2 \int_S w_i w^*_{i(1)}\,\mathrm{d}S \\ -\rho h\omega^2 \int_S (d + w_r) w^*_{r(1)}\,\mathrm{d}S \\ -\rho h\omega^2 \int_S w_i w^*_{i(2)}\,\mathrm{d}S \\ -\rho h\omega^2 \int_S (d + w_r) w^*_{r(2)}\,\mathrm{d}S \end{bmatrix}. \tag{43}$$

The coefficients of the right-hand-side vector are calculated by integration of the actual and virtual deflections of the plate. Therefore, the unknown quantities are very simply obtained by solving the linear system. Obviously, this can only be performed if the matrix can be inverted, that is, the linear equations are independent. This depends on the mechanical configuration (actual fields) and on the choice of the virtual fields. This issue will not be addressed here, but a recent procedure based on the so-called ''special'' virtual fields [30–32] has been shown to solve this problem, provided that the system is linear, which is the case here. It must also be pointed out that this identification procedure is direct. No initial values for the unknown parameters and no iterative process are required.

### 2.9. Simplified identification

In this section, the frequency of the driving movement is chosen to obtain a resonant response of the plate. Full-field measurements provide the real and imaginary components of the deflection and curvature fields of the plate. The same assumptions are made as in Section 2.7 about, respectively, the predominant and negligible contributions of the resonant and non-resonant modes.

#### 2.9.1. Simplified identification of the stiffnesses

In these conditions, Eq. (39) applies. As for the general case, two virtual fields can be chosen and lead to the very simple linear system containing two equations with the stiffnesses as unknowns:

$$\begin{bmatrix} G^{(1)}_{i,i} & H^{(1)}_{i,i} \\ G^{(2)}_{i,i} & H^{(2)}_{i,i} \end{bmatrix} \cdot \begin{bmatrix} D_{xx} \\ D_{xy} \end{bmatrix} = \begin{bmatrix} -\rho h\omega^2 \int_S w_i w^*_{i(1)}\,\mathrm{d}S \\ -\rho h\omega^2 \int_S w_i w^*_{i(2)}\,\mathrm{d}S \end{bmatrix}. \tag{44}$$

These equations are similar, in the isotropic case, to those used in the identification of the stiffnesses of composite anisotropic plates already performed by Grédiac et al. [12,13] by means of the vibrating responses of plates in free–free boundary conditions. The accuracy of the results obviously depends on the above assumption on the resonant mode. Nevertheless, the results

obtained by Grédiac et al. were quite satisfactory, showing that this simplified formulation can be useful in practice.

*2.9.2. Simplified identification of the damping factor*

In this part, it is assumed that the material of the plate presents an isotropic proportional damping such that

$$\beta = \frac{B_{xx}}{D_{xx}} = \frac{B_{xy}}{D_{xy}}. \tag{45}$$

Introducing the preceding expression (45) in Eqs. (38) and (39), these can be rewritten as

$$\beta(D_{xx}G_{i,r} + D_{xy}H_{i,r}) = -\rho h\omega \int_S (d + w_r)w_r^* \mathrm{d}S, \tag{46}$$

$$D_{xx}G_{i,i} + D_{xy}H_{i,i} = -\rho h\omega^2 \int_S w_i w_i^* \,\mathrm{d}S. \tag{47}$$

One can choose a virtual displacement field $w^*(x,y) = w_r^*(x,y) + \mathrm{j}w_i^*(x,y)$ such that $w_r^*(x,y) = w_i^*(x,y)$, so that $G_{i,r} = G_{i,i}$ and $H_{i,r} = H_{i,i}$. Introducing these equalities in Eqs. (46) and (47), we get

$$\beta = \frac{1}{\omega} \cdot \frac{\int_S (d + w_r)w_r^* \,\mathrm{d}S}{\int_S w_i w_i^* \,\mathrm{d}S}. \tag{48}$$

This expression leads to a very simple method to identify the damping factor of a material. Measurements of only the in-phase and $\pi/2$ lag deflection fields of the vibrating plate are needed, which are much easier to perform than measurements of the curvatures. Obviously, the assumption that there is no significant contribution of the non-resonant modes is a limitation for the general application of this procedure. The effect of coupling between modes due to the damping must remain negligible. It would be the case for low damped plates exhibiting well-separated modal frequencies.

## 3. Simulation—identification at resonances

### *3.1. Introduction*

The objective of this section is to check the validity of the method and its robustness (sensitivity to noise). Finite element simulations of isotropic damped plates clamped at one point, as shown in Fig. 1, have been performed. An initial undamped modal analysis provided the first natural frequencies and mode shapes. Then, the forced vibration responses of the plate to sine driving displacements of the clamping point have been computed. This provided the real and imaginary components of the responses of the damped plate for several values of damping. These data are considered as input data to the identification procedure and the corresponding stiffness and damping components are extracted and compared to the reference ones.

Table 1
Parameters of the FE models

| $L$ (mm) | $l$ (mm) | $h$ (mm) | $x_0$ (mm) | $y_0$ (mm) | $\rho$ (kg m$^{-3}$) | $E$ (GPa) | $v$ | $d$ (mm) |
|---|---|---|---|---|---|---|---|---|
| 200 | 100 | 1 | 50 | 25 | 7800 | 210 | 0.3 | 0.1 |

Table 2
Reference stiffness and damping parameters

| | $D_{xx}$ (N m) | $D_{xy}$ (N m) | $B_{xx}$ (N m s) | $B_{xy}$ (N m s) |
|---|---|---|---|---|
| Low damping | 19.2308 | 5.7692 | $1.92 \times 10^{-4}$ | $5.77 \times 10^{-5}$ |
| High damping | 19.2308 | 5.7692 | $1.92 \times 10^{-2}$ | $5.77 \times 10^{-3}$ |

### 3.2. Finite element models

The numerical simulations described below have been carried out using the ANSYS 5.5 finite element package. The theory of the method has been established without any assumption about the shape of the plate. For the sake of simplicity, rectangular plates have been used here, but any other shape could have been chosen. The numerical parameters of the models are reported in Table 1. The definitions of the geometrical data $L$, $l$, $h$, $x_0$ and $y_0$ refer to Fig. 1. As expected, $\rho$, $E$ and $v$ are, respectively, the material density, Young's modulus and Poisson's ratio. It is recalled that $d$ is the amplitude of the driving movement. The FE models are built up using rectangular four-noded Shell63 elements. This element has six degrees of freedom at each node and has both bending and membrane capabilities. For the calculations of the harmonic responses, the damping is introduced by means of a unique $\beta$ proportional damping factor:

$$\beta = \frac{B_{xx}}{D_{xx}} = \frac{B_{xy}}{D_{xy}}. \tag{49}$$

It is important to note that the identification procedure, in the general case, considers the two damping components $B_{xx}$ and $B_{xy}$ to be independent. Therefore, the identification procedure will provide these two values, whether independent or not. Two values of damping have been used for the simulations: the first one, called "low damping", has a value $\beta = 10^{-5}$ and corresponds roughly to the material dissipation of aluminium. The second one, referred to as "high damping", has a value $\beta = 10^{-3}$, which is the damping exhibited by some polymers.

Table 2 presents the reference values of stiffness and damping for, respectively, the low and high damped models of the plate.

### 3.3. Harmonic responses

#### 3.3.1. Presentation

All the simulated data come from calculations with a regular mesh containing 4608 ($48 \times 96$) elements. Figs. 2 and 3 present the harmonic responses calculated respectively with low damping

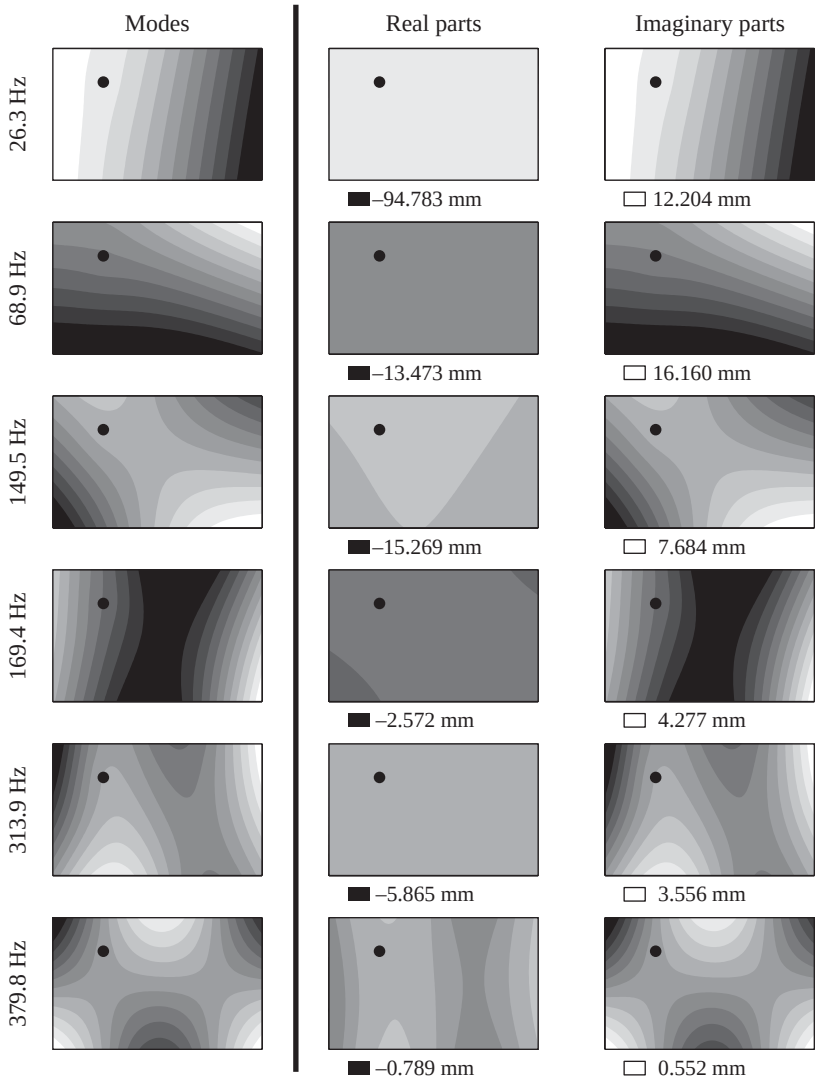


Fig. 2. Plate with low damping. Mode shapes, real and imaginary parts of the responses.

and high damping. In each figure, the central and right-hand-side columns show the shapes of the real and imaginary parts of the responses to an harmonic excitation. The frequencies of the latter are each chosen very close to the frequency of one of the six first modes. For comparisons, the left-hand-side column presents the corresponding mode shapes of the undamped plates. Obviously, each line refers to the same frequency. The modes are drawn with arbitrary scales. For the sake of legibility of the figures, no scale bars are drawn for the responses. Real and imaginary parts referring to the same frequency are drawn with the same grey scale. The black and white colours refer, respectively, to the minimum and maximum deflections and the corresponding values are indicated under each representation.

On each window the black circle mark locates the clamping point.

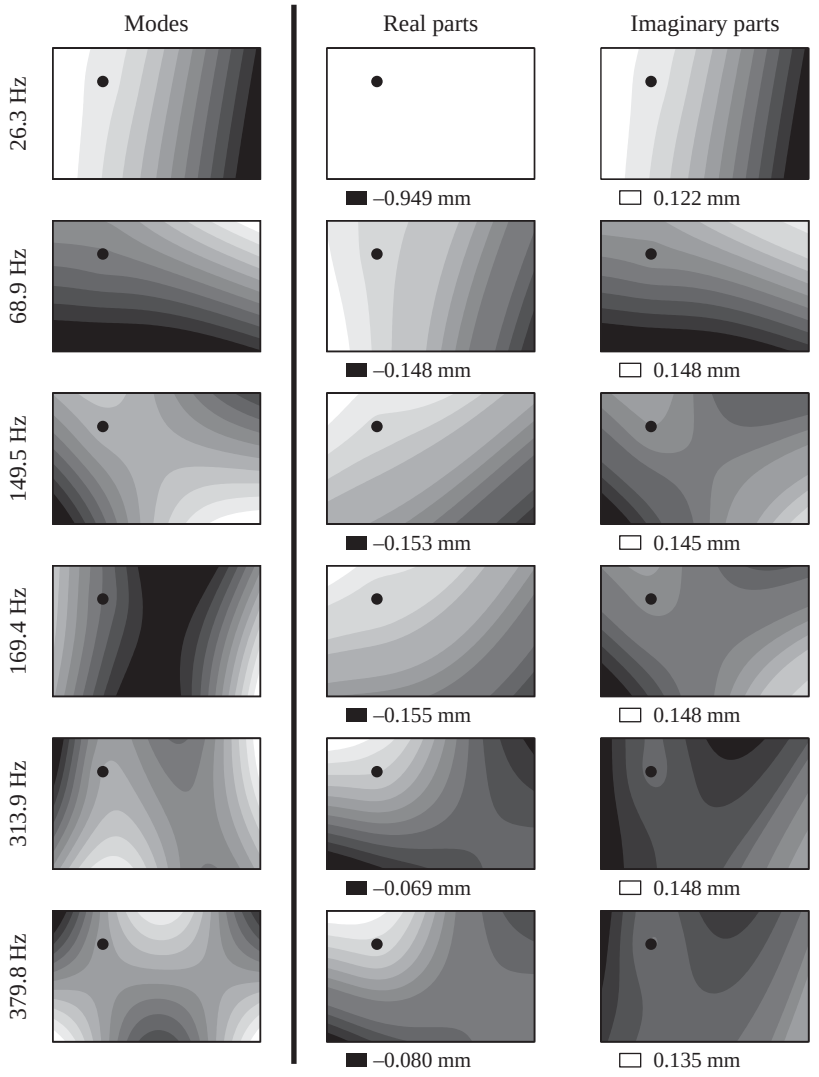


Fig. 3. Plate with high damping. Mode shapes, real and imaginary parts of the responses.

### *3.3.2. Interpretation*

As expected for the low damped plate, the imaginary responses show very sharp resonances with large amplitudes of displacement and shapes very close to the modal ones. This confirms that the resonant mode is predominant for these six cases of excitation and that the damping has no significant coupling effect between modes, i.e. the contributions of the non-resonant modes remain small. In the case of the highly damped plate, for all frequencies, the amplitudes of the real and imaginary parts of the operational deflection shapes remain of the same order of magnitude. Considering the responses in increasing frequency order, one could see that the imaginary parts of the responses are less and less similar to the corresponding mode shapes and the real parts are

Table 3
Plate with low damping—reference general identification with $u_1^*$ and $u_2^*$

| | Freq. (Hz) | | | | | |
|---|---|---|---|---|---|---|
| | 26.4 | 68.9 | 149.5 | 313.9 | 379.8 | 531.0 |
| Rel. err. $D_{xx}$ (%) | −0.01 | −0.04 | −0.02 | −0.05 | −0.36 | −0.20 |
| Rel. err. $D_{xy}$ (%) | −0.02 | −0.05 | 0.01 | −0.01 | −0.10 | −0.63 |
| Rel. err. $B_{xx}$ (%) | −0.01 | −0.03 | 0.08 | 0.07 | 0.61 | 13.64 |
| Rel. err. $B_{xy}$ (%) | −0.02 | −0.05 | 0.03 | 0.17 | −0.69 | 4.06 |

Table 4
Plate with high damping—reference general identification with $u_1^*$ and $u_2^*$

| | Freq. (Hz) | | | | | |
|---|---|---|---|---|---|---|
| | 26.4 | 68.9 | 149.5 | 313.9 | 379.8 | 531.0 |
| Rel. err. $D_{xx}$ (%) | −0.01 | −0.04 | −0.11 | −0.10 | −0.07 | −0.05 |
| Rel. err. $D_{xy}$ (%) | −0.02 | −0.02 | 0.16 | 0.13 | −0.39 | −0.71 |
| Rel. err. $B_{xx}$ (%) | −0.01 | −0.02 | −0.00 | −0.01 | −0.02 | 0.02 |
| Rel. err. $B_{xy}$ (%) | −0.02 | −0.02 | 0.14 | 0.13 | 0.16 | 0.07 |

more and more significant. This is clearly an effect of the viscous proportional damping that increases with the excitation frequency, and the coupling effect increases accordingly.

### 3.4. Reference results—general identification

Tables 3 and 4 show, respectively, the identification results for plates with low and high damping in terms of relative errors between the identified and reference values. Two simple deflection virtual fields are used for this purpose: $u_1^* = d + x^2(1 + \mathrm{j})$ and $u_2^* = d + y^2(1 + \mathrm{j})$.

The results are very good, except for the low damped plate at the highest frequency. This confirms the feasibility of the technique and proves that the virtual fields chosen are suitable enough to extract the unknown parameters.

### 3.5. Reference results—simplified identification

The $2 \times 2$ linear system of Eq. (44) and the simplified equation (48) are used with the simulated responses and the two virtual fields: $u_1^* = d + x^2(1 + \mathrm{j})$ and $u_2^* = d + y^2(1 + \mathrm{j})$, which exhibit identical real and imaginary parts according to the assumption necessary to derive Eq. (48).

Tables 5 and 6 show the results, respectively, for the low and highly damped plates. The $****$ marks are reported when the identification leads to unrealistic results.

In the first case, since the damping effects are low, at resonance the stiffness forces balance the inertial ones. Therefore, correct identifications of the stiffness components are possible. In the case of high damping and because of the coupling effect, there is not the same balance and the

Table 5
Plate with low damping—reference simplified identification with $u_1^*$ and $u_2^*$

| | Freq. (Hz) | | | | | |
|---|---|---|---|---|---|---|
| | 26.4 | 68.9 | 149.5 | 313.9 | 379.8 | 531.0 |
| Rel. err. $D_{xx}$ (%) | −0.01 | −0.04 | 0.01 | −0.12 | −0.36 | 0.55 |
| Rel. err. $D_{xy}$ (%) | −0.02 | −0.04 | −0.00 | −0.18 | 0.12 | 1.53 |
| Rel. err. $\beta$ (%) | −0.22 | **** | **** | **** | **** | **** |

Table 6
Plate with high damping—reference simplified identification with $u_1^*$ and $u_2^*$

| | Freq. (Hz) | | | | | |
|---|---|---|---|---|---|---|
| | 26.4 | 68.9 | 149.5 | 313.9 | 379.8 | 531.0 |
| Rel. err. $D_{xx}$ (%) | −0.05 | 14.18 | **** | **** | **** | **** |
| Rel. err. $D_{xy}$ (%) | −1.15 | **** | **** | **** | **** | **** |
| Rel. err. $\beta$ (%) | −0.96 | **** | **** | **** | **** | **** |

identification generally leads to unrealistic results. However, since the damping used here is proportional, it has a smaller effect at low frequency, which is the reason why the identification performed at the first resonance leads to correct results.

### 3.6. Stability with respect to measurement noise

Since the present procedure will be used in experimental applications, it is necessary to check its stability with respect to noise provided by the measurement set-up. For this purpose, random perturbations from normal distributions have been added to each element curvature and deflection independently. The level of the perturbations has been chosen as 15% of the peak-to-peak values of the corresponding curvatures and deflections. The presented results are the averages of 30 calculations, each time with a new set of noisy data, using the same two virtual fields $u_1^* = d + x^2(1 + j)$ and $u_2^* = d + y^2(1 + j)$. It must be pointed out that this is a rather crude approach to noise simulation, but the purpose here is just to illustrate the stability features of the method. More elaborate simulations will be carried out in the future, using the methodology developed in Ref. [33]. Moreover, the experimental implementation presently underway will enable to characterize more accurately the nature of the noise and, therefore, to better simulate its effect on the identified parameters.

#### 3.6.1. General identifications with noise

Tables 7 and 8 report the coefficients of variation of the identified components respectively for the low and highly damped plates. It can be seen that the method is rather stable, particularly when the damping is high. It must be emphasized here that the sensitivity to noise will be reduced by using the optimized special virtual fields developed in Ref. [33].

Table 7
Plate with low damping—general identification with noise, using $u_1^*$ and $u_2^*$

| | Freq. (Hz) | | | | | |
|---|---|---|---|---|---|---|
| | 26.4 | 68.9 | 149.5 | 313.9 | 379.8 | 531.0 |
| C. var. $D_{xx}$ (%) | 1.36 | 5.65 | 1.73 | 1.14 | 13.72 | 20.12 |
| C. var. $D_{xy}$ (%) | 2.84 | 16.11 | 3.21 | 2.24 | 24.82 | 23.80 |
| C. var. $B_{xx}$ (%) | 1.30 | 17.98 | 8.07 | 12.86 | 29.09 | **** |
| C. var. $B_{xy}$ (%) | 2.87 | **** | 17.77 | **** | **** | **** |

Table 8
Plate with high damping—general identification with noise, using $u_1^*$ and $u_2^*$

| | Freq. (Hz) | | | | | |
|---|---|---|---|---|---|---|
| | 26.4 | 68.9 | 149.5 | 313.9 | 379.8 | 531.0 |
| C. var. $D_{xx}$ (%) | 1.57 | 2.90 | 5.29 | 4.54 | 6.58 | 8.27 |
| C. var. $D_{xy}$ (%) | 3.16 | 5.93 | 15.54 | 13.11 | **** | **** |
| C. var. $B_{xx}$ (%) | 1.49 | 7.27 | 4.81 | 2.64 | 3.51 | 4.62 |
| C. var. $B_{xy}$ (%) | 2.79 | 24.06 | 15.88 | 14.25 | 15.29 | 14.10 |

Table 9
Plate with low damping—simplified identification with noise, using $u_1^*$ and $u_2^*$

| | Freq. (Hz) | | | | | |
|---|---|---|---|---|---|---|
| | 26.4 | 68.9 | 149.5 | 313.9 | 379.8 | 531.0 |
| C. var. $D_{xx}$ (%) | 1.72 | 6.81 | 1.57 | 0.95 | 19.46 | 18.81 |
| C. var. $D_{xy}$ (%) | 3.00 | 19.38 | 3.48 | 1.82 | 32.51 | 26.40 |
| C. var. $\beta$ (%) | 0.08 | **** | **** | **** | **** | **** |

Table 10
Plate with high damping—simplified identification with noise, using $u_1^*$ and $u_2^*$

| | Freq. (Hz) | | | | | |
|---|---|---|---|---|---|---|
| | 26.4 | 68.9 | 149.5 | 313.9 | 379.8 | 531.0 |
| C. var. $D_{xx}$ (%) | 1.72 | **** | **** | **** | **** | **** |
| C. var. $D_{xy}$ (%) | 3.00 | **** | **** | **** | **** | **** |
| C. var. $\beta$ (%) | 0.08 | **** | **** | **** | **** | **** |

*3.6.2. Simplified identifications with noise*

Using the same data as in Section 4.4, simplified identifications of stiffness components and damping factor were attempted with Eqs. (44) and (48).

Tables 9 and 10 show, respectively, the results corresponding to the low and highly damped plates.

The results for the first one remain correct concerning the stiffness components. They confirm the experimental results obtained in Refs. [12,13] using carbon/epoxy composite plates that exhibit moderate damping.

In the future, it would be interesting to investigate the domain of applicability of the simplified approach leading to Eq. (48). Indeed, in this case, only deflection measurements are needed which are easier to perform than curvature measurements. The simplified approach could therefore be a very useful, simple and robust method to measure damping on slender panels.

## 4. Simulation—identification out of resonances

### *4.1. Introduction*

Since the complex expression of the harmonic responses introduced in Section 2.1 needs no particular assumption, it remains valid for any frequency of excitation. Therefore, Eqs. (34) and (33) set in Section 2.6 must be verified at resonance and out of resonance so that using linear system (43) derived from these equations, identification of stiffness and damping is possible out of resonance.

### *4.2. Simulated harmonic responses*

Figs. 4 and 5 show, respectively, for the low damped and highly damped plates, the real and imaginary parts of the operational deflection shapes of the plate due to harmonic excitation of six equally spaced frequencies.

In the same manner as in the previous Figs. 2 and 3, the central and right-hand-side columns show the real and imaginary parts of the responses with the same scale on each line. The minimum and maximum values of deflections, respectively, associated to black and white colours, are reported under each line. The corresponding excitation frequencies are indicated between the two columns. The first six mode shapes are recalled in the left-hand-side column with associated resonance frequencies.

It is interesting to note that, for the low damped plate (Fig. 4), the real response is predominant over the imaginary response, except for the third frequency, because it is close to a resonance frequency of the undamped plate, so that this mode is nearly resonant. This is also the reason why the shape of the imaginary part of the response is nearly the same as the corresponding mode. Since the damping is low, there is no significant contribution of the non-resonant modes in the vicinity of the resonance, whereas the phase variation of the response is very sharp. Since the excitation frequency is not exactly the resonance frequency, the phase of the response is not $\pi/2$, which explains that the response has significant real and imaginary components with the same patterns.

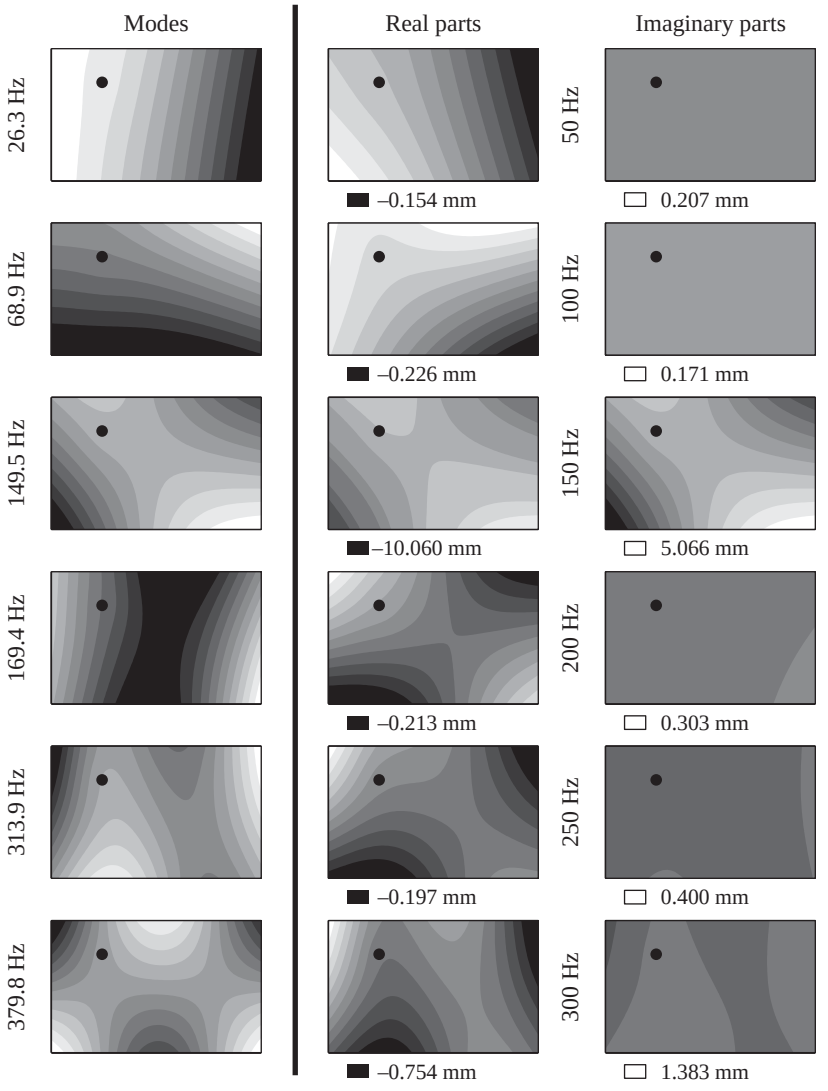


Fig. 4. Plate with low damping. Excitation out of resonance. Real and imaginary parts of the responses.

On the contrary, in Fig. 5, because of the high damping effects, the contribution of the non-resonant modes is significant and the shape of the real response to the third excitation frequency is quite different from the imaginary one.

### 4.3. Reference results

The following results come from calculations with the entry data provided by finite element simulations.

Tables 11 and 12 report the identification results out of resonance, respectively, for the low and highly damped plate using the following virtual fields: $u_1^*$ and $u_2^*$.

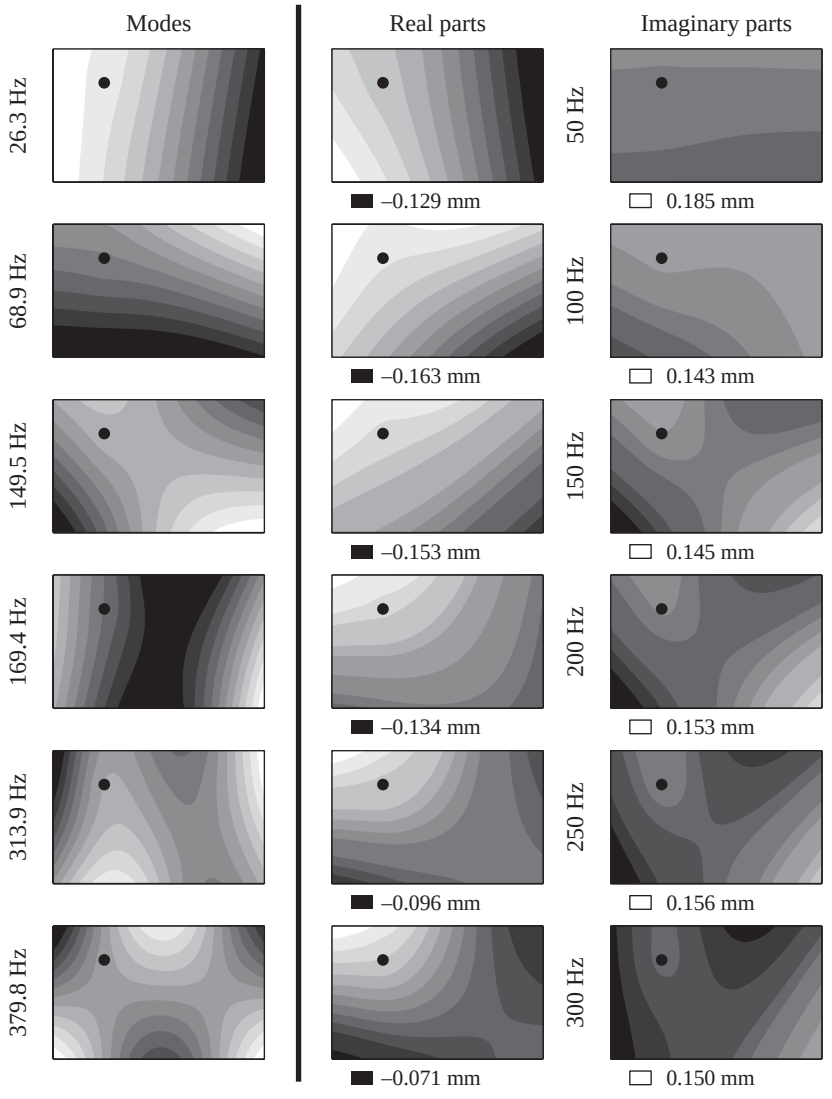


Fig. 5. Plate with high damping. Excitation out of resonance. Real and imaginary parts of the responses.

It can be seen that all unknowns are identified correctly, except for the damping parameters for the second frequency and the low damped plate. Again, it is confirmed that it is easier to identify the damping in the case of the highly damped plate, which is what was expected.

### 4.4. Results with noisy data

The stability of the identification out of resonance has been tested with the same procedure as that described in section. Tables 13 and 14 show the results for, respectively, the low and highly damped plates, using the following virtual fields: $u_1^*$ and $u_2^*$. As for the results reported in section, it can be seen that the results are satisfactory for the high damping but poor for the low damping.

Table 11
Plate with low damping—reference identifications out of resonances, using $u_1^*$ and $u_2^*$

| | Freq. (Hz) | | | | | |
|---|---|---|---|---|---|---|
| | 50 | 100 | 150 | 200 | 250 | 300 |
| Rel. err. $D_{xx}$ (%) | −0.02 | −0.25 | −0.02 | −0.02 | −0.07 | −0.29 |
| Rel. err. $D_{xy}$ (%) | −0.00 | −0.75 | 0.01 | 0.15 | 0.14 | −0.15 |
| Rel. err. $B_{xx}$ (%) | −0.02 | 3.54 | 0.10 | 0.55 | −0.46 | 0.34 |
| Rel. err. $B_{xy}$ (%) | −0.04 | 12.07 | 0.03 | 1.85 | −1.77 | −0.46 |

Table 12
Plate with high damping—reference identifications out of resonances, using $u_1^*$ and $u_2^*$

| | Freq. (Hz) | | | | | |
|---|---|---|---|---|---|---|
| | 50 | 100 | 150 | 200 | 250 | 300 |
| Rel. err. $D_{xx}$ (%) | −0.02 | −0.06 | −0.11 | −0.10 | −0.10 | −0.08 |
| Rel. err. $D_{xy}$ (%) | −0.01 | −0.02 | 0.16 | 0.07 | −0.09 | −0.32 |
| Rel. err. $B_{xx}$ (%) | −0.01 | −0.00 | −0.00 | −0.02 | −0.03 | −0.02 |
| Rel. err. $B_{xy}$ (%) | −0.03 | 0.14 | 0.14 | 0.17 | 0.20 | 0.18 |

Table 13
Plate with low damping—identifications with noise out of resonances, using $u_1^*$ and $u_2^*$

| | Freq. (Hz) | | | | | |
|---|---|---|---|---|---|---|
| | 50 | 100 | 150 | 200 | 250 | 300 |
| C. var. $D_{xx}$ (%) | 3.47 | 16.52 | 1.14 | 20.45 | 52.49 | 16.46 |
| C. var. $D_{xy}$ (%) | 10.17 | **** | 2.82 | **** | **** | **** |
| C. var. $B_{xx}$ (%) | 5.31 | **** | **** | **** | **** | **** |
| C. var. $B_{xy}$ (%) | 25.18 | **** | **** | **** | **** | **** |

Table 14
Plate with high damping—identifications with noise out of resonances, using $u_1^*$ and $u_2^*$

| | Freq. (Hz) | | | | | |
|---|---|---|---|---|---|---|
| | 50 | 100 | 150 | 200 | 250 | 300 |
| C. var. $D_{xx}$ (%) | 2.74 | 2.75 | 4.07 | 5.01 | 6.50 | 7.13 |
| C. var. $D_{xy}$ (%) | 8.12 | 7.65 | 14.78 | 16.35 | 19.57 | **** |
| C. var. $B_{xx}$ (%) | 2.99 | 4.00 | 3.89 | 2.60 | 2.54 | 3.33 |
| C. var. $B_{xy}$ (%) | 13.75 | 8.32 | 14.19 | 11.49 | 11.84 | 11.98 |

Table 15
Plate with low damping—identifications with noise out of resonances, using $u_1^*$ and $u_4^*$

| | Freq. (Hz) | | | | | |
|---|---|---|---|---|---|---|
| | 50 | 100 | 150 | 200 | 250 | 300 |
| C. var. $D_{xx}$ (%) | 5.25 | 23.19 | 1.05 | **** | **** | 23.90 |
| C. var. $D_{xy}$ (%) | 21.65 | **** | 3.89 | **** | **** | **** |
| C. var. $B_{xx}$ (%) | 19.71 | **** | **** | **** | **** | **** |
| C. var. $B_{xy}$ (%) | **** | **** | **** | **** | **** | **** |

Table 16
Plate with high damping—identifications with noise out of resonances, using $u_1^*$ and $u_4^*$

| | Freq. (Hz) | | | | | |
|---|---|---|---|---|---|---|
| | 50 | 100 | 150 | 200 | 250 | 300 |
| C. var. $D_{xx}$ (%) | 2.56 | 2.36 | 2.30 | 2.86 | 4.37 | 4.58 |
| C. var. $D_{xy}$ (%) | 9.78 | 7.68 | 8.09 | 9.81 | 15.71 | 17.00 |
| C. var. $B_{xx}$ (%) | 3.40 | 2.95 | 1.53 | 1.77 | 2.42 | 2.32 |
| C. var. $B_{xy}$ (%) | 13.69 | 10.34 | 5.28 | 6.37 | 8.49 | 8.38 |

Table 17
Plate with low damping—identifications with noise out of resonances, using $u_3^*$ and $u_4^*$

| | Freq. (Hz) | | | | | |
|---|---|---|---|---|---|---|
| | 50 | 100 | 150 | 200 | 250 | 300 |
| C. var. $D_{xx}$ (%) | 5.80 | 24.39 | 0.87 | 22.57 | **** | 25.24 |
| C. var. $D_{xy}$ (%) | 26.05 | **** | 2.97 | **** | **** | **** |
| C. var. $B_{xx}$ (%) | 16.78 | **** | **** | **** | **** | **** |
| C. var. $B_{xy}$ (%) | **** | **** | **** | **** | **** | **** |

Table 18
Plate with high damping—identifications with noise out of resonances, using $u_3^*$ and $u_4^*$

| | Freq. (Hz) | | | | | |
|---|---|---|---|---|---|---|
| | 50 | 100 | 150 | 200 | 250 | 300 |
| C. var. $D_{xx}$ (%) | 3.53 | 2.72 | 1.84 | 2.70 | 4.05 | 5.70 |
| C. var. $D_{xy}$ (%) | 13.26 | 8.87 | 6.01 | 9.22 | 15.04 | 21.95 |
| C. var. $B_{xx}$ (%) | 6.64 | 4.07 | 2.28 | 2.11 | 2.21 | 2.04 |
| C. var. $B_{xy}$ (%) | 21.03 | 13.66 | 7.67 | 7.82 | 7.87 | 6.76 |

Since these results are highly dependent on the choice of the virtual fields, two other combinations of virtual fields have been tried. Tables 15 and 16 report the results obtained with $u_1^* = d + x^2(1 + j)$ and $u_4^* = d + xy(1 + j)$, and Tables 17 and 18, that obtained with $u_3^* = d + x^2 + jy^2$ and $u_4^* = d + xy(1 + j)$. No significant improvement can be seen, although small differences exist. The next step is to use optimized virtual fields as defined in Ref. [33].

## 5. Conclusion

The present paper is the first attempt at proposing a novel procedure to derive both stiffness and damping parameters from forced vibrating isotropic plates. The key feature is that displacement and curvature fields can be measured at different times over the whole surface of the plate by a suitable optical technique. As a consequence, the virtual fields method (VFM) provides sets of equations relating the stiffness and damping parameters to these measured fields and to geometric and excitation (frequency, amplitude) parameters.

The main advantage of the present method is that it does not rely on strong assumptions on the response of the plate and can even be applied out of resonance. It is also independent of the shape of the plate. In particular, it can be a very powerful tool to investigate the frequency dependence of damping for a wide range of materials. It is also interesting to note that simplified formulae have been obtained to derive the damping ratio as a function of the deflection field only. This approach is very attractive and its domain of applicability will have to be more closely investigated.

In the future, the extension of the present approach to anisotropic plates will be performed, in order to test fibre composites or laminates used as panels in the bodies of vehicles. The numerical performance of the method will be increased by adopting the latest developments of the VFM [33] and by designing optimized test configurations in the same spirit as in Ref. [34], but using a different technique based on the sensitivity indicators in Ref. [33]. Finally, the experimental implementation of the technique is underway using a deflectometry technique (slope measurements) based on the reflection of a grid in the tested plate [35,36]. Preliminary results have shown the feasibility of this technique for application on vibrating plates [37].

## Acknowledgements

The authors would like to thank Professor Michel Grédiac for useful discussions about the use of the Virtual Fields Method in dynamics.

## References

[1] C. Horgan, Saint-Venant end effects in composite structures, *Composites Engineering* 3 (1994) 279–286.
[2] Y. Arimitsu, K. Nishioka, T. Senda, A study of Saint-Venant's principle for composite materials by means of internal stress fields, *Journal of Applied Mechanics* 62 (1995) 53–58.

[3] F. Pierron, E. Alloba, Y. Surrel, A. Vautrin, Whole-field assessment of the effects of boundary conditions on the strain field in off-axis tensile testing of unidirectional composites, *Composites Science and Technology* 58 (12) (1998) 1939–1947.
[4] P. Pedersen, Optimization method applied to identification of material parameters, in: H.A. Eschenauer, G. Thierauf (Eds.), *Discretization Methods and Structural Optimization—Procedures and Applications*, Springer, Berlin, 1989.
[5] P. Pedersen, P.S. Frederiksen, Identification of orthotropic materials moduli by combinated experimental numerical approach, *Measurements* 10 (1992) 113–118.
[6] P. Frederiksen, Identification of elastic constants including transverse shear moduli of thick orthotropic plates, Tech. rep., Danish Centre for Applied Mathematics and Mechanics, report number 500, 1995.
[7] P.S. Frederiksen, Numerical studies for identification of orthotropic elastic constants of thick plates, *European Journal of Mechanics A/Solids* 16 (1997) 117–140.
[8] H. Sol, Identification of Anisotropic Plate Rigidities using Free Vibration Data, Ph.D. thesis, Free University of Brussels, 1986.
[9] J. Cunha, J. Piranda, Application of model updating techniques in dynamics for the identification of elastic constants of composite materials, *Composites, Part B* 30 (1999) 79–85.
[10] L. Deobald, R. Gibson, Determination of elastic constants of orthotropic plates by a modal analysis/Rayleigh–Ritz technique, *Journal of Sound and Vibration* 124 (2) (1988) 269–283.
[11] E. Ayorinde, R. Gibson, Elastic constants of orthotropic composite materials using plate resonance frequencies, classical lamination theory and an optimized three-mode Rayleigh formulation, *Composites Engineering* 3 (5) (1993) 395–407.
[12] M. Grédiac, P.-A. Paris, Direct identification of elastic constants of anisotropic plates by modal analysis: theoretical and numerical aspects, *Journal of Sound and Vibration* 193 (3) (1996) 401–415.
[13] M. Grédiac, N. Fournier, P.-A. Paris, Y. Surrel, Direct determination of elastic constants of anisotropic plates by modal analysis: experimental results, *Journal of Sound and Vibration* 210 (5) (1998) 643–659.
[14] Y. Surrel, N. Fournier, M. Grédiac, P.-A. Paris, Phase-stepped deflectometry applied to shape measurement of bent plates, *Experimental Mechanics* 39 (1) (1998) 66–70.
[15] R. Gibson, Modal vibration response measurements for characterization of composite materials and structures, *Composites Science and Technology* 60 (2000) 2769–2780.
[16] G. Wren, V. Kinra, On the effect of an end-mass on a beam damping, *Experimental Mechanics* 9 (1989) 336–341.
[17] G. Wren, V. Kinra, Modeling and measurement of axial and flexural damping in metal-matrix composites, in: *Mechanics and Mechanisms of Material Damping*, vol. 1169, American Society for Testing and Materials, 1992, pp. 282–315.
[18] G. Wren, V. Kinra, Flexural damping of a p55 graphite magnesium composite, *Journal of Materials Science* 30 (1995) 3279–3284.
[19] J. Bishop, V. Kinra, Some improvements in the flexural damping measurement techniques, in: *Mechanics and Mechanisms of Material Damping*, vol. 1169, American Society for Testing and Materials, 1992, pp. 457–470.
[20] I. Finegan, R. Gibson, Recent research on enhancement of damping in polymer composite, *Composite Structures* 44 (1999) 89–98.
[21] R. Gibson, Damping characteristics of composites materials and structures, *Journal of Materials Engineering and Performance* 1 (1992) 11–20.
[22] Z. Zhang, G. Hartwig, Relation of damping and fatigue damage of unidirectional fibre composite, *International Journal of Fatigue* 24 (2002) 713–718.
[23] D. Ouis, Effect of structural defects on the strength and damping properties of a solid material, *European Journal of Mechanics A/Solids* 22 (2003) 47–54.
[24] N. Srikanth, M. Gupta, Damping characterization of magnesium based composites using an innovative circle-fit approach, *Composites Science and Technology* 63 (2003) 559–568.
[25] R. Gibson, R. Plunkett, Dynamic behavior of fiber-reinforced composites: measurements and analysis, *Journal of Composite Materials* 10 (1976) 325–332.
[26] V. Jiejun, L. Chenggong, W. Dianbin, G. Manchang, Damping and sound absorption properties of particle al matrix composite foams, *Composites Science and Technology* 63 (2003) 569–574.

[27] A. Giraudeau, F. Pierron, J.-P. Chambard, Experimental study of air effect on vibrating lightweight structures, in: *SEM Annual Congress on Experimental Mechanics*, Society for Experimental Mechanics, 10–12 June 2002, Milwaukee, USA.
[28] E. Toussaint, M. Grédiac, F. Pierron, The virtual fields method with piecewise virtual fields, *International Journal of Mechanical Sciences, Submitted.*.
[29] I. Doghri, *Mechanics of Deformable Solids*, Springer, 2000.
[30] M. Grédiac, E. Toussaint, F. Pierron, Special virtual fields for the direct determination of material parameters with the virtual fields method. 1—principle and definition, *International Journal of Solids and Structures* 39 (10) (2000) 2691–2705.
[31] M. Grédiac, E. Toussaint, F. Pierron, Special virtual fields for the direct determination of material parameters with the virtual fields method. 2—application to in-plane properties, *International Journal of Solids and Structures* 39 (10) (2002) 2707–2730.
[32] M. Grédiac, E. Toussaint, F. Pierron, Special virtual fields for the direct determination of material parameters with the virtual fields method. 3—application to the bending rigidities of anisotropic plates, *International Journal of Solids and Structures* 40 (10) (2003) 2401–2419.
[33] S. Avril, M. Grédiac, F. Pierron, Sensitivity of the virtual fields method to noisy data, *Computational Mechanics* 34 (6) (2004) 439–452.
[34] L. LeMagorou, F. Bos, F. Rouger, Identification of constitutive laws for wood-based panels by means of an inverse method, *Composites Science and Technology* 62 (4) (2002) 591–596.
[35] Y. Surrel, Deflectometry: a simple and efficient noninterferometric method for slope measurement, in: *Xth SEM International Congress on Experimental Mechanics*, Society for Experimental Mechanics, 2004.
[36] S. Avril, E. Toussaint, M. Grédiac, F. Pierron, Y. Surrel, Deflectometry and virtual fields for identification of static plate bending stiffnesses, in: *Xth SEM International Congress on Experimental Mechanics*, Society for Experimental Mechanics, 2004.
[37] A. Giraudeau, B. Guo, F. Pierron, Identification of stiffness and damping material properties from forced vibrating plates, in: *12th International Conference on Experimental Mechanics*, 2004.